Rab11a mediates cell-cell spread and reassortment of influenza A virus genomes via tunneling nanotubes.

Ketaki Ganti[1], Julianna Han[2#], Balaji Manicassamy[3], Anice C. Lowen[1,4*]*

1 Department of Microbiology and Immunology, Emory University School of Medicine, Atlanta, GA, USA

2 Department of Microbiology, University of Chicago, Chicago, IL, USA

3 Department of Microbiology and Immunology, University of Iowa School of Medicine, Iowa City, IA, USA

4 Emory-UGA Centers of Excellence for Influenza Research and Surveillance (CEIRS)

Current address: Department of Integrative Structural and Computational Biology, The Scripps Research Institute, La Jolla, CA, USA

*Corresponding Authors

Email: ketaki.ganti@emory.edu; anice.lowen@emory.edu

Abstract:

Influenza A virus (IAV) genomes comprise eight negative strand RNAs packaged into virions in the form of viral ribonucleoproteins (vRNPs). Rab11a plays a crucial role in the transport of vRNPs from the nucleus to the plasma membrane via microtubules, allowing assembly and virus production. Here, we identify a novel function for Rab11a in the inter-cellular transport of IAV vRNPs using tunneling nanotubes (TNTs) as molecular highways. TNTs are F-Actin rich tubules that link the cytoplasm of nearby cells. In IAV-infected cells, Rab11a was visualized together with vRNPs in these actin-rich intercellular connections. To better examine viral spread via TNTs, we devised an infection system in which conventional, virion-mediated, spread was not possible. Namely, we generated HA-deficient reporter viruses which are unable to produce progeny virions but whose genomes can be replicated and trafficked. In this system, vRNP transfer to neighboring cells was observed and this transfer was found to be dependent on both actin and Rab11a. Generation of infectious virus via TNT transfer was confirmed using donor cells infected with HA-deficient virus and recipient cells stably expressing HA protein. Mixing donor cells infected with genetically distinct IAVs furthermore revealed the potential for Rab11a and TNTs to serve as a conduit for genome mixing and reassortment in IAV infections. These data therefore reveal a novel role for Rab11a in the IAV life cycle, which could have significant implications for within-host spread, genome reassortment and immune evasion.

41

42 **Author Summary:**

43 Influenza A viruses infect epithelial cells of the upper and lower respiratory tract in humans.
44 Infection is propagated by the generation of viral particles from infected cells, which
45 disseminate within the tissue. Disseminating particles can encounter obstacles in the
46 extracellular environment, including mucus, ciliary movement, antibody neutralization and
47 uptake by phagocytic immune cells. An alternative mode of spread, which avoids these hazards,
48 involves direct transport of viral components between cells. This cell-cell spread of infection is
49 not a well understood process. In this study we demonstrate that the host factor Rab11a
50 mediates the transport of viral genomes in the cell-cell spread of infection. Rab11a is already
51 known to play a pro-viral role in the transport of viral genomes to the plasma membrane for
52 assembly into virus particles. Here, we see that this same transport mechanism is co-opted for
53 direct cell-cell spread through cellular connections called tunneling nanotubes. We show that
54 complexes of Rab11a and viral components can be trafficked across tunneling nanotubes,
55 transmitting infection without the formation of virus particles. Importantly, this route of spread
56 often seeds viral genomes from multiple donor cells into recipient cells, which in turn increases
57 viral genetic diversity.

58 **Introduction:**

59 Influenza A virus (IAV) genomes are composed of eight RNA segments that are packaged into
60 the virion in the form of viral ribonucleoproteins (vRNPs), which contain viral nucleoprotein
61 (NP) as well as the polymerase complex (PB2, PB1 and PA) (1). Influenza genome packaging

62 mechanisms have been studied extensively and, although there are a lot of unknowns, it has
63 been demonstratively shown that the host cell protein Rab11a is crucial for the trafficking of
64 newly synthesized vRNPs after they exit the nucleus to the site of assembly at the plasma
65 membrane (2,3). Rab11a is a small GTPase that has multiple roles in the host cell, including a
66 pivotal role in retrograde transport of cargo on recycling endosomes (4,5). The intracellular
67 transport of vRNP-Rab11a complexes is thought to occur via the microtubule network with the
68 help of dynein motors (6–11), and disruption of this network by nocodazole has been shown to
69 attenuate the generation of viral progeny (8). Similarly, our prior work revealed that loss of
70 Rab11a reduces infectious viral titers, most likely due to a defect in the packaging of vRNPs,
71 leading to the formation of incomplete viral particles (12). Taken together, these data
72 demonstrate the importance of an intact microtubule network as well as Rab11a in the IAV life
73 cycle.

74 Tunneling nanotubes (TNTs) are F-Actin rich cellular connections that are formed between two
75 or more cells (13). These connections can be formed over long distances and provide
76 cytoplasmic connectivity between the cells, allowing for exchange of materials including
77 organelles, nutrients, and membrane vesicles (14–16). Many viruses including HIV (17–19),
78 herpesviruses (20) and IAVs (21,22) have been shown to utilize these TNTs for cell-cell spread.
79 Previous work has shown that IAV spread via TNTs proceeds in the presence of neutralizing
80 antibodies or antivirals such as oseltamivir (21,22). This mode of infection does not depend on
81 the formation of viral particles, thus allowing for the assembly stage of the lifecycle to be
82 bypassed. Although the use of TNTs by IAVs has been demonstrated, the exact mechanism is
83 unclear.

84 In this study, we show that Rab11a mediates the transport of IAV vRNPs and proteins through
85 TNTs, as evidenced by Rab11a co-localization with viral components in TNTs and the disruption
86 of this transport with Rab11a knock out. This system was observed to be functional in multiple
87 host cell backgrounds and virus strains. Using HA deficient viruses, we confirm that transport of
88 viral components through TNTs can seed productive infection in recipient cells. In the context
89 of viral co-infection, we find direct cell-cell spread often seeds viral genomes from multiple
90 donor cells into recipient cells, thus promoting genome mixing and reassortment. Finally, our
91 data suggest that, at least in the case of IAV infection, TNTs access the cytosol of both
92 connected cells and allow bi-directional movement of cargo. Taken together, these findings
93 demonstrate a novel and crucial role for Rab11a in the trafficking of IAV genomes via tunneling
94 nanotubes and extend mechanistic understanding of this unconventional mode of viral
95 dissemination.

96 **Results:**

97 ***IAV vRNPs associate with Rab11a within F-Actin rich TNTs.***

98 Upon nuclear exit, IAV vRNPs bind to Rab11a via PB2, allowing their transport to the plasma
99 membrane for assembly (8,23,24). We hypothesized that vRNP-Rab11a complexes could also be
100 routed to F-Actin rich intercellular connections called tunneling nanotubes (TNTs) and could
101 seed new infections by direct transport through TNTs. To test this hypothesis, we visualized
102 Rab11a, F-Actin and viral nucleoprotein (NP) - as a marker for vRNPs - in MDCK cells infected
103 with either influenza A/Netherlands/602/2009 (NL09; pH1N1) or A/Panama/2007/99 (P99;
104 H3N2) virus. NP and Rab11a were seen to co-localize in a perinuclear compartment, as has

105 been shown previously (2,9). In addition, co-localization of these components was observed
106 within the F-Actin rich TNTs connecting infected and uninfected cells (Fig 1A and Supp Fig 1).
107 This observation suggests that there are at least two functional pathways for the trafficking of
108 vRNP-Rab11a complexes post nuclear exit: the canonical assembly pathway and the TNT-
109 mediated genome transfer pathway.

110 To further corroborate the role of Rab11a in the transport of vRNPs across TNTs, we used
111 Rab11a knockout (KO) A549 cells generated by CRISPR/Cas9 (12) and wild type (WT) A549 cells
112 as a control. As before, cells were infected with either NL09 or P99 viruses and then stained for
113 NP, Rab11a and F-Actin. WT cells showed co-localization of NP and Rab11a in the perinuclear
114 region and within TNTs (Fig 1B and Supp Fig 1). Conversely, Rab11a KO cells did not show NP
115 staining within the TNTs, indicating that Rab11a drives the transfer of vRNPs through TNTs (Fig
116 1C and Supp Fig 1).

117 We used super resolution Stimulated Emission Depletion (STED) microscopy to analyze the
118 association of Rab11a and vRNPs within TNTs in more detail. STED microscopy overcomes the
119 diffraction resolution limit of confocal microscopy and allows for imaging with up to 30 nm
120 resolution (25,26). A549 WT or Rab11a KO cells were infected with NL09 viruses and stained
121 for NP, Rab11a and F-Actin. Using 3 color STED imaging of TNTs, we observed punctate Rab11a
122 and NP staining in close proximity within the TNTs in WT cells. In the case of the Rab11a KO
123 cells, the NP staining was relatively diffuse in the cytoplasm and could not be observed within
124 the TNTs (Figure 2A). Co-localization of Rab11a and NP within TNTs was analyzed quantitatively
125 for both WT and KO cells. The observed colocalization co-efficient of 0.9 in the WT cells
126 indicates that the majority of the NP puncta within TNTs coincide with Rab11a puncta (Figure

127 2B). These data indicate that Rab11a and NP are indeed interacting with each other within TNTs
128 and are likely trafficked as a complex.

129 To evaluate the frequency with which Rab11a accesses TNTs, we quantified the percentage of
130 TNTs that were NP+Rab11a+, NP+Rab11a- and NP-Rab11a+ in uninfected and NL09 infected
131 A549 WT cells. Rab11a was routinely detected within the TNTs of uninfected cells, indicating
132 that Rab11a+ recycling endosomes are trafficked within TNTs under normal conditions (Figure
133 2C). In infected cells, a majority of TNTs carried NP+Rab11a+ puncta, indicating that transport
134 of vRNPs into TNTs is a common feature of the viral life cycle (Figure 2C).

135 ***Rab11a does not modulate TNT formation.***

136 IAV infection increases the number of TNTs formed between cells (21,22). To test whether the
137 loss of Rab11a had an impact on TNT formation, we counted the number of TNTs formed
138 between cells in WT and Rab11a KO cells in the presence and absence of NL09 infection.
139 Consistent with prior work, a significant increase in the number of TNTs formed upon IAV
140 infection was observed in both WT and KO cells (Figure 3). Conversely, we saw no significant
141 difference between WT and KO cells in the number of TNTs formed, either in the context of
142 infection or mock infection (Figure 3). The observation that loss of Rab11a does not significantly
143 impact TNT formation suggests that the reliance of vRNP trafficking through TNTs on Rab11a
144 arises through the observed interaction between these components.

145 ***Disruption of actin or loss of Rab11a significantly attenuates direct cell-cell transmission of***
146 ***infection***.

147 Since we observed the presence of vRNP-Rab11a complexes within TNTs, we next tested
148 whether the loss of either the TNTs or Rab11a influences the cell-cell spread of IAV infection.
149 Previously, neutralizing antibodies or neuraminidase inhibitors have been used to block
150 conventional viral infection and allow examination of IAV protein and RNA transport via TNTs
151 (21,22). Although these methods are effective in abrogating conventional spread, we wanted to
152 fully eliminate the generation of viral progeny to define the role of Rab11a and TNTs in IAV
153 genome transfer more clearly. To this end, we rescued recombinant viruses in the NL09 and
154 P99 strain backgrounds that lack the HA gene but instead contain either mVenus (NL09 ΔHA
155 Venus; P99 ΔHA Venus) or mScarlet (NL09 ΔHA Scarlet) fluorescent reporter ORFs flanked by HA
156 packaging signals. These HA deficient reporter viruses are infection competent but are unable
157 to produce progeny in the absence of a HA complementing cell line. Therefore, these viruses
158 are excellent tools to study the cell-cell spread of IAV infection via TNTs.

159 To analyze the role of F-actin in the cell-cell spread of viral genomes, MDCK cells were infected
160 with either NL09 ΔHA Venus or P99 ΔHA Venus viruses in the presence or absence of
161 Cytochalasin D, which is a potent inhibitor of actin polymerization and disrupts TNTs (21,22).
162 Cytochalasin D was added 2 h post internalization. HA positive cells were counted at 16, 24, and
163 48 h post-infection (p.i.) and binned into one of two categories: single cells or foci comprising
164 >=2 contiguous, positive cells. We hypothesized that the disruption of TNTs by Cytochalasin D
165 would severely limit the spread of IAV genomes from infected cells, preventing the formation of
166 infected foci. As shown in Figure 4A and B, there was a significant reduction in the number of
167 infected foci in the Cytochalasin D treated cells compared to the untreated controls in both the

168 NL09 ΔHA Venus and P99 ΔHA Venus infected cells. These data confirm that intact TNTs are
169 required for direct cell-cell spread of IAV genetic material.

170 Next, we analyzed the role of Rab11a in direct cell-cell spread of IAV. To do this, A549 WT and
171 Rab11a KO cells were infected with either NL09 ΔHA Venus or P99 ΔHA Venus viruses. Venus
172 positive cells were counted at 16, 24, and 48 h p.i. and categorized based on their presence as
173 single cells or within foci at each time point. If Rab11a directs transport of vRNPs across TNTs,
174 the loss of Rab11a would be expected to reduce the cell-cell spread of IAV genetic material. As
175 shown in Figure 4C and D, this was indeed the case. In contrast to WT controls, the number of
176 infected foci did not increase over time in the Rab11 KO cells. These data provide further
177 evidence for the role of Rab11a in this alternate infection pathway.

178 ***Virion-independent genome transfer leads to productive infection by an actin-dependent***
179 ***mechanism.***

180 To assess whether all eight genome segments can be transported via TNTs leading to the
181 production of infectious progeny, we performed a co-culture experiment using MDCK cells and
182 a MDCK-derived cell line which expresses the HA of influenza A/WSN/33 (H1N1) virus on the
183 cell surface (MDCK WSN HA cells). When infected with an HA deficient reporter virus, these
184 cells provide the HA protein required for the generation of infectious virus particles. For
185 subsequent analysis of co-infection via TNT/Rab11a mediated genome transfer, these
186 experiments were set up using two IAV strains, NL09 ΔHA Venus WT and NL09 ΔHA Scarlet VAR
187 viruses. In addition to carrying differing reporter genes, these viruses differ in the presence of a

188 silent mutation in each segment of the VAR virus, which acts as a genetic tag (27). Neither of
189 these differences is important for the purposes of the present analysis.

190 As outlined in Figure 5A, separate dishes of MDCK cells were singly infected with either NL09
191 ΔHA Venus WT or NL09 ΔHA Scarlet VAR virus. After infection for 2 hours, the cells were acid
192 washed to remove residual inoculum and then trypsinized to make a cell slurry. MDCK cells
193 infected with NL09 ΔHA Venus WT and NL09 ΔHA Scarlet VAR were mixed with naïve MDCK
194 WSN HA cells in the ratio 1:1:2. The cell mixture was plated in medium containing trypsin (to
195 allow activation of HA) and ammonium chloride (to prevent secondary infections mediated by
196 virus particles). If all eight segments of the viral genome can be transported across TNTs to a
197 conducive cell, which in this case must be a MDCK WSN HA cell, then the recipient cell will
198 produce virus particles. To detect any such progeny viruses produced, supernatant was
199 collected at 0, 24, 48 and 72 h post mixing and plaque assays were performed on MDCK WSN
200 HA cells.

201 To evaluate the role of TNTs in cell-cell spread of infection, cells were treated with either
202 vehicle or 30 µM Cytochalasin D, which disrupts F-Actin. As can be seen from Figure 5B,
203 infectious virus was detected in the vehicle treated control cells, but not in the Cytochalasin D
204 treated cells. Virus production in vehicle treated cells demonstrates the transfer of the full
205 complement of IAV genome segments from infected cells, which lack HA protein and cannot
206 produce virions, to cells which express complementing HA protein. A lack of virus production in
207 Cytochalasin D treated cells indicates that this transfer was F-Actin-dependent, strongly
208 implicating TNTs. Comparing the two MOIs tested (2.5 and 25 PFU/cell), a dose dependence

209 was observed at 24 h, which is most likely due to the increased probability of an infected cell
210 making a connection with a naïve MDCK WSN HA cell at higher MOI.

211 To assess if actin depolymerization was impairing vRNP transport upstream of TNT transfer, we
212 tested the effect of Cytochalasin D on conventional virus production in the context of multicycle
213 replication. No difference in viral yield from vehicle treated or Cytochalasin D treated cells was
214 detected (Figure 5C). Taken together, these data indicate that actin depolymerization
215 specifically abrogates TNT mediated transfer of viral genomes but has no impact on
216 conventional viral assembly.

217 To test if microtubules play a role in TNT mediated transport of IAV genomes, we performed
218 the co-culture assay as described above with vehicle treated and 30 µM Nocodazole, which
219 depolymerizes microtubules. We detected infectious virus in both control and nocodazole
220 treated cells (Figure 5D), indicating that microtubules most likely did not play a role in the
221 trafficking of vRNPs through TNTs.

222 Finally, to analyze the effect of the loss of Rab11a on the production of infectious progeny, we
223 co-cultured either A549 WT or A549 Rab11a KO cells infected with the NL09 ΔHA Venus WT or
224 NL09 ΔHA Scarlet VAR viruses with the MDCK WSN HA complementing line as described above.
225 Supernatant was collected at 24, 48 and 72 h post mixing and plaque assays were performed on
226 MDCK WSN HA cells. As can be seen from Figure 5E, infectious virus was detected from both
227 A549 WT and Rab11a KO cells, with a marginal difference in titers. Since this observation was
228 incongruent with our previous data demonstrating the importance of Rab11a in the transport
229 of vRNPs, we hypothesized the transfer of viral genomes from the Rab11a KO cells was

230 occurring via Rab11a that originates in the MDCK WSN HA cells. If correct, this observation
231 would indicate that TNTs are open ended and allow for bi-directional movement of cargo.

232 ***TNTs allow bidirectional shuttling of Rab11a between cells***

233 To analyze if Rab11a could shuttle form one cell to another in a bi-directional manner, we used
234 A549 WT and Rab11a KO cells in combination. Briefly, A549 Rab11a KO cells were infected with
235 NL09 WT virus. The infected cells were then mixed in a 1:1 ratio with uninfected A549 WT cells
236 which were pre-stained with CellTracker Blue dye. The mixed cells were stained for NP, Rab11a
237 and F-Actin at 24h post-mixing and imaged using STED microscopy. We observed NP and
238 Rab11a within the TNTs connecting the infected KO cells and the uninfected WT cells (Figure
239 6A). Co-localization analysis again showed Rab11a-NP colocalization within TNTs in this KO-WT
240 co-culture system (Figure 6B), although the coefficient was lower than that seen in a fully
241 Rab11a competent system (Figure 2B). Since the WT cell is the only source of Rab11a in the KO-
242 WT co-culture, our data show that Rab11a traveling from an uninfected cell to an infected cell
243 can pick up vRNPs. The production of viral progeny observed in this system further indicates
244 that this Rab11a from the originally uninfected cell can then transport vRNPs back through the
245 TNTs, mediating infection. Our data suggest that TNTs formed in the context of IAV infection
246 are open ended and likely bi-directional.

247 ***TNTs serve as conduits for genome mixing and reassortment.***

248 Since we observed that infectious progeny could be generated via Rab11a-mediated genome
249 transfer through TNTs, we hypothesized that this process could also mediate co-infection and
250 therefore reassortment. In particular, reassortment would be expected if differentially infected

251 donor cells connect to the same recipient cell. To test this hypothesis, the genotypes of virus
252 produced from the co-cultures described in Figure 5E were evaluated. In these experiments,
253 cells infected with NL09 ΔHA Venus WT virus were mixed with cells infected with NL09 ΔHA
254 Scarlet VAR virus and these infected cells were in turn mixed with MDCK WSN HA cells; thus,
255 co-infections could occur if WT infected and VAR infected cells each formed connections with
256 the same HA-expressing recipient cell and a full complement of IAV segments was reconstituted
257 therein. The silent mutations differentiating each of the non-HA gene segments of the WT and
258 VAR viruses allow the parental origin of segments to be identified. Thus, to evaluate
259 reassortment, plaque clones were isolated from co-culture supernatants and the genotype of
260 each was determined. The results show that viruses generated from MDCK WSN HA cells mixed
261 with infected A549 WT cells were predominantly reassortant under all conditions evaluated
262 (Figure 7A). In contrast, when MDCK WSN HA cells were mixed with infected A549 Rab11 KO
263 cells, parental viruses typically dominated (Figure 7B). Thus, in a Rab11a-sufficient system,
264 intercellular transfer of IAV vRNPs through TNTs readily yielded reassortants, indicating that
265 TNTs are forming a network rather than pairwise connections between cells. When Rab11a was
266 absent from infected donor cells, however, reassortants were rarely observed. Since Rab11a
267 knock out does not impact the number of TNTs formed (Figure 3), this relative lack of
268 reassortants suggests that vRNP transport through TNTs is less efficient when Rab11a is absent
269 from donor cells.

270 We note that, in both data sets shown in Figure 7, richness of viral genotypes was low, with at
271 most four distinct gene constellations detected in each sample of 21 plaque isolates. This
272 observation suggests that very few cells are producing most of the progeny virus in this

273 experimental system, and that each producer cell is releasing virus with only one or a small
274 number of genotypes. In turn, this suggests that MDCK WSN HA cells that receive a full
275 complement of IAV vRNPs do not tend to receive multiple copies of a given segment. Although
276 low in both culture systems, richness was significantly higher in the samples derived from A549
277 WT cells compared to those from A549 Rab11a KO cells, with 2.8 and 1.9 unique genotypes
278 detected on average, respectively (p=0.019, t-test). This difference is consistent with less
279 efficient vRNP transfer when donor cells lack Rab11a.

280 **Discussion:**

281 Our data reveal a novel role for the host GTPase Rab11a in the trafficking of IAV genomes via
282 tunneling nanotubes. We decisively show that productive infection can be mediated through
283 this direct cell-to-cell route and find evidence that Rab11a can move through TNTs in a
284 bidirectional manner to mediate IAV genome transfer. In the context of mixed infections, we
285 furthermore find that TNT/Rab11a-mediated transfer readily leads to cellular coinfection and
286 reassortment.

287 The trafficking of IAV genomes is a complex and poorly understood process. Although it is
288 known that newly synthesized vRNPs form transient complexes with active Rab11a post nuclear
289 exit and are trafficked to the plasma membrane for assembly on microtubule structures (6–9),
290 the fate of these complexes is not completely elucidated. Here we examined the potential for
291 Rab11a-vRNP complexes to be trafficked through TNTs to neighboring cells. Tunneling
292 nanotubes (TNTs) are F-Actin based cytoplasmic connections that are utilized for long distance
293 communication and have been shown to have a role in the IAV life cycle (21,22). TNTs can be

294 used to transport vesicular cargo (14,28–30), so we posed the question of whether the Rab11a-
295 vRNP vesicular complexes could be re-routed to these structures. We show that Rab11a and
296 vRNPs co-localize within TNTs in multiple cell types, with near complete concordance of NP
297 with Rab11a in high resolution STED images of TNTs. Loss of Rab11a leads to severely reduced
298 detection of NP within the TNTs and more dispersed NP localization within the cytoplasm.
299 These observations strongly suggest that Rab11a-vRNP complexes are transported within TNTs.

300 TNTs are mainly composed of F-Actin and the transport of organelles through TNTs requires
301 myosin motor activity on actin filaments (11,23–25). Since Rab11a can utilize both dynein
302 motors, which drive microtubule movement (6,26,27), and myosin motors, which drive actin
303 dynamics (28–30), the observation that Rab11a mediates transport through TNTs raises the
304 question of which motor proteins are involved. Studies to date on IAV infection have mainly
305 focused on the role of Rab11a and microtubules. Further studies are needed to determine
306 whether the same transport mechanism is active within TNTs and, conversely, whether Rab11a-
307 actin dynamics may function in vRNP transport both within and between cells. Although Rab11a
308 has been shown to be important for trafficking and efficient assembly of IAV genomes (2,8,12),
309 we have shown that the loss of Rab11a does not completely abrogate genome assembly and
310 viral particle release, indicating that there may exist an alternative pathway for canonical
311 assembly of virions (12).

312 We observed that infectious progeny could be recovered from co-cultures of infected Rab11a
313 KO A549 cells with MDCK WSN HA cells, which was incongruous with our previous observation
314 that Rab11a KO abrogated the cell-cell transmission of infection. We were able to resolve this
315 paradox by utilizing high-resolution STED imaging to visualize the transport of Rab11a from

316 uninfected A549 WT cells to infected A549 Rab11a KO cells, where vRNPs could be picked up
317 and trafficked through TNTs. TNTs can be formed in multiple ways - single ended, open ended
318 or closed - and therefore support varying modes of transport (13,16,31). The generation of
319 progeny virions in the Rab11a KO co-culture is likely due to the formation of open ended, bi-
320 directional TNTs that allow Rab11a from the HA-expressing producer cell to shuttle to and from
321 infected KO cells where it could pick up vRNPs. This process seems to be inefficient, however,
322 as evidenced by the low rate of reassortment observed when infected cells do not encode
323 Rab11a. Bi-directional transfer of organelles such as mitochondria through TNTs have been
324 observed in various cell types, including lung mesothelioma cells (32). It is also possible that
325 there exists another host factor that can mediate vRNP transport through TNTs in the absence
326 of Rab11a, albeit inefficiently. The possibility of bidirectional trafficking of vRNPs between cells,
327 or potential novel host factors involved in vRNP transport, opens hitherto unexplored avenues
328 of viral infection.

329 Our data revealing that coinfection and reassortment can occur through TNT transfer of vRNPs
330 between cells raise new questions about the processes driving IAV genetic exchange. The
331 prevalence of reassortants produced via TNT transfer from Rab11a+ cells indicates that vRNPs
332 may be trafficked individually or as subgroups and not as a constellation of 8 segments. This
333 process would then seed incomplete viral genomes into recipient cells, which require
334 complementation to allow the production of progeny viruses. Owing to this reliance on
335 complementation, incomplete viral genomes are known to augment reassortment (33–35). Our
336 data suggest that both seeding and complementation of incomplete viral genomes can occur
337 via TNT transfer of vRNPs. In the presence of a conventional viral infection system, co-infection

338 with multiple virions is thought to be the *modus operandi* of IAV reassortment, where
339 reassortment efficiency is a function of the dose and relative timing of two infections, as well as
340 levels of incomplete viral genomes (27,33). It will be interesting to determine whether TNT-
341 mediated co-infection is also sensitive to dose and timing. More broadly, further work is
342 needed to tease out the extent to which TNT mediated reassortment occurs alongside
343 conventional modes of reassortment.

344 The human airway is composed of multiple cell types, including polarized epithelial cells in a
345 tightly packed environment (36). It is yet unclear what role TNTs may play in the normal
346 homeostasis of the airway, but TNTs have been demonstrated to mediate the transfer of cargo
347 and organelles in various solid tumors of the lung, including adenocarcinomas and
348 mesotheliomas (32). TNT mediated transfer of organelles and other components including
349 viruses has been observed between heterotypic cells, mostly involving immune cells such as
350 macrophages (37–40). It is therefore likely that IAV infection of the airway epithelium or
351 potentially immune cells can spread via TNTs *in vivo*. The extent to which TNT mediated spread
352 acts in conjunction with particle-based transmission of infection within the host is as yet
353 unexplored. IAV spread through TNTs may be particularly important in the evasion of
354 antibodies, and other antiviral factors that act directly on extracellular virions, in a manner that
355 does not depend on the generation of escape mutants. It has been recently shown that cell-cell
356 spread of H5N1 influenza viruses can occur via trogocytosis in which there is an exchange of the
357 plasma membrane and its associated molecules between conjugated cells (41). This mechanism
358 is also actin dependent and is potentially another route of HA-independent direct cell-cell
359 spread of infection. Direct cell-cell spread may also make an important contribution to spatial

360 structure within the infected host, leading to more localized spread and limiting mixing among
361 *de novo* variants (42). To further investigate these potential implications, an exciting prospect
362 for future work is the development of *ex vivo* and *in vivo* models for the study and visualization
363 of TNT mediated cell-cell spread.

364 In summary, our data show a novel role for Rab11a in the IAV life cycle, where it can mediate
365 vesicular transport of vRNPs across TNTs and seed new infections (Figure 8). Future work to
366 elucidate the exact mechanism of transport of the Rab11a-vRNP complexes, including the
367 motors utilized and the fate of the incoming Rab11a-vRNP complexes in the recipient cytosol,
368 are exciting avenues to be studied and will further our understanding of IAV-host interactions.

369 **Materials and Methods:**

370 *Cells and cell culture media*

371 MDCK cells (obtained from Dr. Daniel Perez) and MDCK WSN HA cells (obtained from Dr. Ryan
372 Langlois) were maintained Minimal Essential Medium (Sigma) supplemented with 10% fetal
373 bovine serum (FBS; Atlanta Biologicals), penicillin (100 IU ml^{-1}), and streptomycin
374 (100 µg ml^{-1}; PS; Corning). A549 WT, A549 Rab11a KO were maintained in Dulbecco's
375 Modified Essential Medium (Gibco) supplemented with 10% FBS (Atlanta Biologicals), and PS.
376 All cells were cultured at 37 °C and 5% CO_2 in a humidified incubator. All cell lines were tested
377 monthly for mycoplasma contamination while in use. The medium for culture of IAV in each cell
378 line (termed virus medium) was prepared by eliminating FBS and supplementing the
379 appropriate medium with 4.3% BSA and PS. Ammonium chloride-containing virus medium was

380 prepared by the addition of HEPES buffer and NH_4Cl at final concentrations of 50 mM and 20
381 mM, respectively. OPTi-MEM (Gibco) was used as a serum free medium where indicated.

382 *Generation of Rab11a KO Cells*

383 Generation and characterization of Rab11a KO A549 cells was reported in (12,43). Briefly, two
384 guide RNAs (gRNA) targeting the promoter and exon 1 of the Rab11a gene were used.
385 Oligonucleotides for the CRISPR target sites T1 (forward CACCGCATTTCGAGTAAATCGAGAC and
386 reverse AAACGTCTCGATTTACTCGAAATGC) and T2 (forward CACCGTAACATCAGCGTAAGTCTCA
387 and reverse AAACTGAGACTTACGCTGATGTTAC) were annealed and cloned into lentiCRISPRv2
388 (Addgene #52961) and LRG (Addgene #65656) expression vectors, respectively. A549 cells
389 transduced with lentivirus vectors expressing gRNAs were selected in the presence of 2 μg/mL
390 puromycin for 10 days and clonal Rab11a KO cells were generated by limiting dilution of the
391 polyclonal population. Rab11a KO cells were identified by PCR analysis of the targeted genomic
392 region using the following primers (forward TGTTCAACCCCCTACCCCCATTC and reverse
393 TGGAAGCAAACACCAGGAAGAACTC) and further confirmed by western blot analysis of Rab11a
394 expression (43).

395 *Viruses*

396 All viruses used in this study were generated by reverse genetics (44). For influenza
397 A/Panama/2007/99 virus (P99; H3N2), 293T cells transfected with reverse-genetics plasmids
398 16–24 h previously were injected into the allantoic cavity of 9- to 11-d-old embryonated
399 chicken eggs and incubated at 37 °C for 40–48 h. The resultant egg passage 1 stocks were used
400 in experiments. For influenza A/Netherlands/602/2009 virus (NL09; pH1N1), 293T cells

401 transfected with reverse-genetics plasmids 16–24 h previously were co-cultured with MDCK
402 cells at 37 °C for 40–48 h. The supernatants were then propagated in MDCK cells at a low MOI
403 to generate NL09 working stocks. The titers for these viruses were obtained by plaque assays
404 on MDCK cells.

405 The NL09 ΔHA Venus WT, P99 ΔHA Venus WT and NL09 ΔHA Scarlet VAR viruses were
406 generated by reverse genetics by co-culture with MDCK WSN HA cells rather than MDCK cells.
407 The ΔHA Venus and ΔHA Scarlet rescue plasmids were prepared by inserting either the mVenus
408 (45) or mScarlet (46) ORF within the HA sequence, retaining only the 3' terminal 136
409 nucleotides of the HA segment upstream of the reporter gene start codon and the 5' terminal
410 136 nucleotides of the HA segment downstream of the reporter gene stop codon. ATG
411 sequences within the upstream portion were mutated to ATT to prevent premature translation
412 start (47). As previously described (48), one silent mutation was introduced into each NL09
413 cDNA to generate the NL09 VAR reverse genetics system, which was used to generate the NL09
414 ΔHA Scarlet VAR virus. These silent mutations enable differentiation of VAR virus segments
415 from those of the WT virus using high-resolution melt analysis (27,49).

416 *Immunofluorescence and Confocal Imaging*

417 For fixed cell imaging, MDCK, A549 WT or A549 Rab11a KO cells were seeded onto glass
418 coverslips. Infection with either NL09 or P99 viruses was performed the next day by adding 250
419 µl of inoculum to the coverslips and incubating at 37°C for 1 h with intermittent rocking.
420 Inoculum was removed, cells washed twice with 1X PBS and Opti-MEM added to the dish. After
421 incubation at 37°C for 24 h, cells were washed with 1X PBS (Corning) thrice and fixed with 4%

422 paraformaldehyde (AlfaAesar) for 15 minutes at room temperature. Cells were washed with 1X
423 PBS and permeabilized using 1% Triton X-100 (Sigma) in PBS for 5 minutes at room temperature
424 and washed with 1X PBS. Cells were stained with mouse anti NP antibody (Abcam ab43821)
425 (1:100), rabbit anti Rab11a antibody (Sigma HPA051697) (1:100), and Phalloidin Alexa Fluor 647
426 (Invitrogen A22287) (1:40) overnight at 4°C. Cells were washed thrice with 1X PBS and
427 incubated with donkey anti mouse Alexa Fluor 555 (Invitrogen A32773) (1:1000) and Anti rabbit
428 Alexa Fluor 488 (Invitrogen A32731) (1:1000) for 1 h at 37°C. Coverslips were washed thrice
429 with 1X PBS and mounted on glass slides using ProLong Diamond Anti-Fade Mountant with
430 DAPI (Invitrogen P36962) prior to imaging.

431 Confocal images were collected using the Olympus FV1000 Inverted Microscope at 60X 1.49 NA
432 Oil magnification on a Prior motorized stage. Images were acquired with a Hamamatsu Flash
433 4.0 sCMOS camera controlled with Olympus Fluoview v4.2 software. All images were processed
434 using Fiji image analysis software (50).

435 *Immunofluorescence and High-Resolution STED Imaging*

436 A549 WT or A549 Rab11a KO cells were seeded onto glass coverslips. Infection with NL09 WT
437 viruses was performed the next day by adding 250 µl of inoculum to the coverslips and
438 incubating at 37°C for 1 h with intermittent rocking. Inoculum was removed, cells washed twice
439 with 1X PBS and Opti-MEM added to the dish. After incubation at 37°C for 24 h, cells were
440 washed with 1X PBS (Corning) thrice and fixed with 4% paraformaldehyde (AlfaAesar) for 15
441 minutes at room temperature. Cells were washed with 1X PBS and permeabilized using 1%
442 Triton X-100 (Sigma) in PBS for 5 minutes at room temperature and washed with 1X PBS. Cells

443 were stained with mouse anti NP antibody (Abcam ab43821) (1:50), rabbit anti Rab11a
444 antibody (Proteintech 20229-1-AP) (1:50), and CellMask Deep Red Actin Tracking Stain
445 (Invitrogen A57248) (1:1000) overnight at 4°C. Cells were washed thrice with 1X PBS and
446 incubated with goat anti- mouse STAR ORANGE (Abberior STORANGE-1001) and goat anti-
447 rabbit STAR GREEN (Abberior STGREEN-1002) for 1 h at 37°C. Coverslips were washed thrice
448 with 1X PBS and mounted on glass slides using ProLong Diamond Anti-Fade Mountant with
449 DAPI (Invitrogen P36962) prior to imaging.

450 For the A549 KO-WT co-culture experiment, WT cells were pre-stained with CellTracker Blue
451 CMAC dye (Invitrogen C2110) (1:500) overnight at 37°C in OPTIMEM. This dye stains thiols in
452 the cytoplasm and fluoresces blue under the DAPI filter. Cells were washed with 1X PBS,
453 trypsinized and then mixed with NL09 infected Rab11a KO cells and seeded onto glass
454 coverslips. After incubation at 37°C for 24 h, cells were processed and stained as described
455 above. Coverslips were washed thrice with 1X PBS and mounted on glass slides using ProLong
456 Glass Anti-Fade Mountant (Invitrogen P36980) prior to imaging.

457 Images were taken using an Abberior Facility Line STED microscope, controlled via Lightbox.
458 Single planes were acquired at 900 x 900 px (150 µm × 150 µm) with a 4 µs dwell time and a
459 line accumulation of 4. A 60X NA 1.4 (oil immersion; UPLXAPO60XO) objective lens was used
460 with a confocal pinhole of 0.5 AU. The Alexa 647 STED channel (F-Actin) was excited with a 1
461 mW pulsed 640 nm laser line at 1% and spectral detection at 650–735 nm. 2D STED was
462 induced with a 2750 mW 775nm pulsed laser at 25%. The STAR ORANGE channel (NP) was
463 excited with a 200µW pulsed 561 nm laser line at 10% and spectral detection at 574-637 nm.
464 2D STED was induced with a 2750 mW 775 nm pulsed laser at 25%. The STAR GREEN channel

465 (Rab11a) was excited with a 1mW pulsed485 nm laser line at 5% and spectral detection at 498-
466 574 nm. 2D STED was induced with a 400mW 595 nm pulsed laser at 30%. The DAPI/CellTracker
467 Blue channel was excited with a 20 mW 405 nm laser line at 3% and spectral detection at 415-
468 497 nm. All 2D STED images were acquired at a 2 µs dwell time.

469 *Quantification of co-localization*

470 Co-localization efficiency of NP and Rab11a was calculated using the Manders coefficient (51)
471 with the Costes threshold (52) on both A549 WT and Rab11a KO cells using the JaCoP plugin
472 (53) in FiJi (50).

473 *Quantification of cell-cell transmission*

474 MDCK, A549 WT and A549 KO cells were inoculated with NL09 ΔHA Venus WT or P99 ΔHA
475 Venus WT virus at a MOI of 0.5 PFU/cell and incubated for 1 h at 37°C. Cells were washed with
476 1X PBS (Corning) to remove residual inoculum and supplemented with OPTI-MEM (Gibco)
477 without trypsin and in the presence of 30 µM Cytochalasin D (Sigma) where indicated and
478 incubated at 37°C. Infected cells were counted manually by the presence of green fluorescence
479 using an epifluorescence microscope (Zeiss) at the time points indicated and binned into single
480 infected or foci of infected cells. Foci were defined as clusters of at least two contiguous,
481 positive, cells. The cell counts were graphed using the GraphPad Prism software (54).

482 *Co-culture for production of infectious virus*

483 MDCK, A549 WT or A549 Rab11a KO cells were inoculated with either NL09 ΔHA Venus WT or
484 NL09 ΔHA Venus VAR at a MOI of 25 PFU/cell or 2.5 PFU/cell and were incubated in virus
485 medium without trypsin for 2 h at 37°C. Cells were washed twice with 1X PBS (Corning) and

486 then treated with PBS-HCl, pH 3.0 for 5 min at room temperature to remove residual inoculum.
487 Cells were washed once with 1X PBS and then trypsinized using 0.5 M trypsin-EDTA (Corning).
488 Cell slurry was collected in growth medium containing FBS and centrifuged at 1000 rpm or 5
489 minutes in a tabletop centrifuge (Thermo Sorvall ST16) to pellet cells. Supernatant was
490 aspirated and cells resuspended in virus medium containing TPCK-trypsin (Sigma), 20 mM
491 HEPES (Corning) and 50 mM NH_4Cl (Sigma) with or without 30 µM Cytochalasin D (Sigma) or 30
492 µM Nocodazole (Sigma) as indicated. Infected cell slurry was mixed with naïve MDCK WSN HA
493 cells in a ratio of 1:1:2 of NL09 ΔHA Venus WT: NL09 ΔHA Scarlet VAR: Naïve MDCK WSN HA
494 cells respectively and plated onto 6-well plates. Cells were allowed to attach at 37°C and
495 supernatant was collected at indicated time points for analysis.

496 *Conventional production of infectious virus with Cytochalasin D treatment*

497 MDCK cells were infected with NL09 WT virus at a MOI of 25 PFU/cell, acid washed as described
498 above to remove residual inoculum and incubated with or without 30 µM Cytochalasin D in
499 virus medium containing TPCK-trypsin. Supernatant was collected at indicated time points for
500 analysis.

501 *Quantification of reassortment*

502 Reassortment was quantified for coinfection supernatants as described previously (27). Briefly,
503 plaque assays were performed on MDCK WSN HA cells in 10 cm dishes to isolate virus clones.
504 Serological pipettes (1 ml) were used to collect agar plugs into 160 µl PBS. Using a ZR-96 viral
505 RNA kit (Zymo), RNA was extracted from the agar plugs and eluted in 40 µl nuclease-free water
506 (Invitrogen). Reverse transcription was performed using Maxima reverse transcriptase (RT;

507 ThermoFisher) according to the manufacturer's protocol. The resulting cDNA was diluted 1:4 in
508 nuclease-free water, each cDNA was combined with segment-specific primers (Supplementary
509 Table 1) and Precision melt supermix (Bio-Rad) and analysed by qPCR using a CFX384 Touch
510 real-time PCR detection system (Bio-Rad) designed to amplify a region of approximately 100 bp
511 from each gene segment that contains a single nucleotide change in the VAR virus. The qPCR
512 was followed by high-resolution melt analysis to differentiate the WT and VAR amplicons (27).
513 Precision Melt Analysis software (Bio-Rad) was used to determine the parental virus origin of
514 each gene segment based on the melting properties of the cDNA fragments and comparison to
515 WT and VAR controls. Each plaque was assigned a genotype based on the combination of WT
516 and VAR genome segments, with two variants on each of seven segments allowing for 128
517 potential genotypes.

518 **Acknowledgements:**

519 We thank Drs. Daniel Perez and Ryan Langlois for generous sharing of cell lines. This research
520 project was supported in part by the Emory University Integrated Cellular Imaging Microscopy
521 Core, supported by the Office of the Director, NIH (S10OD028673). The project was funded by
522 NIH/NIAID Centers of Excellence in Influenza Research and Surveillance (CEIRS), contract
523 number HHSN272201400004C and NIH R01AI127799. Julianna Han was partly supported by the
524 NIH Molecular and Cellular Biology training program at The University of Chicago
525 (T32GM007183); Julianna Han was partly supported by the NIH Diversity Supplement
526 (R01AI123359- 02S1). Dr. Balaji Manicassamy is supported by NIAID grants (R01AI123359 and
527 R01AI127775). The content of this article is solely the responsibility of the authors and does not
528 necessarily represent the official views of the National Institutes of Health.

529 **References:**

530 1. Noda T. Selective Genome Packaging Mechanisms of Influenza A Viruses. Cold Spring
531 Harb Perspect Med. 2020;

532 2. Eisfeld AJ, Kawakami E, Watanabe T, Neumann G, Kawaoka Y. RAB11A Is Essential for
533 Transport of the Influenza Virus Genome to the Plasma Membrane. J Virol. 2011;

534 3. Amorim MJ. A comprehensive review on the interaction between the host GTPase Rab11
535 and influenza A virus [Internet]. Vol. 6, Frontiers in Cell and Developmental Biology.
536 Frontiers Media S.A.; 2019 [cited 2021 Jun 9]. p. 176. Available from:
537 www.frontiersin.org

538 4. Weisz OA, Rodriguez-Boulan E. Apical trafficking in epithelial cells: Signals, clusters and
539 motors. Journal of Cell Science. 2009.

540 5. Chen W, Feng Y, Chen D, Wandinger-Ness A. Rab11 is required for trans-Golgi network-
541 to-plasma membrane transport and a preferential target for GDP dissociation inhibitor.
542 Mol Biol Cell. 1998;

543 6. Nturibi E, Bhagwat AR, Coburn S, Myerburg MM, Lakdawala SS. Intracellular
544 Colocalization of Influenza Viral RNA and Rab11A Is Dependent upon Microtubule
545 Filaments. J Virol. 2017;

546 7. Bhagwat AR, Le Sage V, Nturibi E, Kulej K, Jones J, Guo M, et al. Quantitative live cell
547 imaging reveals influenza virus manipulation of Rab11A transport through reduced
548 dynein association. Nat Commun. 2020;

549 8. Amorim MJ, Bruce EA, Read EKC, Foeglein A, Mahen R, Stuart AD, et al. A Rab11- and
550 Microtubule-Dependent Mechanism for Cytoplasmic Transport of Influenza A Virus Viral
551 RNA. J Virol. 2011;

552 9. Bruce EA, Digard P, Stuart AD. The Rab11 Pathway Is Required for Influenza A Virus
553 Budding and Filament Formation. J Virol. 2010;

554 10. De Castro Martin IF, Fournier G, Sachse M, Pizarro-Cerda J, Risco C, Naffakh N. Influenza
555 virus genome reaches the plasma membrane via a modified endoplasmic reticulum and
556 Rab11-dependent vesicles. Nat Commun [Internet]. 2017 Dec 1 [cited 2021 Jun 9];8(1):1–
557 12. Available from: www.nature.com/naturecommunications

558 11. Alenquer M, Vale-Costa S, Etibor TA, Ferreira F, Sousa AL, Amorim MJ. Influenza A virus
559 ribonucleoproteins form liquid organelles at endoplasmic reticulum exit sites. Nat
560 Commun [Internet]. 2019 Dec 1 [cited 2021 Jun 9];10(1):1–19. Available from:
561 https://doi.org/10.1038/s41467-019-09549-4

562 12. Han J, Ganti K, Sali VK, Twigg C, Zhang Y, Manivasagam S, et al. Host factor Rab11a is
563 critical for efficient assembly of influenza A virus genomic segments. PLOS Pathog
564 [Internet]. 2021 May 10 [cited 2021 May 26];17(5):e1009517. Available from:
565 https://pubmed.ncbi.nlm.nih.gov/33970958/

566 13. Austefjord MW, Gerdes HH, Wang X. Tunneling nanotubes: Diversity in morphology and
567 structure. Commun Integr Biol. 2014;

568 14. Gerdes HH, Carvalho RN. Intercellular transfer mediated by tunneling nanotubes. Current

569 Opinion in Cell Biology. 2008.

570 15. Abounit S, Zurzolo C. Wiring through tunneling nanotubes - from electrical signals to
571 organelle transfer. J Cell Sci. 2012;

572 16. Marzo L, Gousset K, Zurzolo C. Multifaceted roles of tunneling nanotubes in intercellular
573 communication. Frontiers in Physiology. 2012.

574 17. Hashimoto M, Bhuyan F, Hiyoshi M, Noyori O, Nasser H, Miyazaki M, et al. Potential Role
575 of the Formation of Tunneling Nanotubes in HIV-1 Spread in Macrophages. J Immunol.
576 2016;

577 18. Bracq L, Xie M, Benichou S, Bouchet J. Mechanisms for cell-to-cell transmission of HIV-1.
578 Frontiers in Immunology. 2018.

579 19. Eugenin E a, Gaskill PJ, Berman JW. A potential mechanism for intercellular HIV
580 trafficking. Commun Integr Biol. 2009;

581 20. Panasiuk M, Rychłowski M, Derewońko N, Bieńkowska-Szewczyk K. Tunneling Nanotubes
582 as a Novel Route of Cell-to-Cell Spread of Herpesviruses. J Virol. 2018;

583 21. Kumar A, Kim JH, Ranjan P, Metcalfe MG, Cao W, Mishina M, et al. Influenza virus
584 exploits tunneling nanotubes for cell-to-cell spread. Sci Rep. 2017;

585 22. Roberts KL, Manicassamy B, Lamb RA. Influenza A Virus Uses Intercellular Connections To
586 Spread to Neighboring Cells. J Virol. 2015;

587 23. Momose F, Sekimoto T, Ohkura T, Jo S, Kawaguchi A, Nagata K, et al. Apical transport of
588 influenza A virus ribonucleoprotein requires Rab11-positive recycling endosome. PLoS

589 One. 2011;

590 24. Avilov S V., Moisy D, Naffakh N, Cusack S. Influenza A virus progeny vRNP trafficking in
591 live infected cells studied with the virus-encoded fluorescently tagged PB2 protein.
592 Vaccine [Internet]. 2012 Dec 7 [cited 2021 Jun 25];30(51):7411–7. Available from:
593 https://pubmed.ncbi.nlm.nih.gov/23063830/

594 25. Hell SW, Wichmann J. Breaking the diffraction resolution limit by stimulated emission:
595 stimulated-emission-depletion fluorescence microscopy. Opt Lett [Internet]. 1994 Jun 1
596 [cited 2021 May 26];19(11):780. Available from:
597 https://pubmed.ncbi.nlm.nih.gov/19844443/

598 26. Klar TA, Jakobs S, Dyba M, Egner A, Hell SW. Fluorescence microscopy with diffraction
599 resolution barrier broken by stimulated emission. Proc Natl Acad Sci U S A [Internet].
600 2000 Jul 18 [cited 2021 May 26];97(15):8206–10. Available from:
601 https://pubmed.ncbi.nlm.nih.gov/10899992/

602 27. Marshall N, Priyamvada L, Ende Z, Steel J, Lowen AC. Influenza Virus Reassortment
603 Occurs with High Frequency in the Absence of Segment Mismatch. PLoS Pathog. 2013;

604 28. Jansens RJJ, Tishchenko A, Favoreel HW. Bridging the Gap: Virus Long-Distance Spread
605 via Tunneling Nanotubes. J Virol. 2020;

606 29. Kimura S, Hase K, Ohno H. Tunneling nanotubes: Emerging view of their molecular
607 components and formation mechanisms. Exp Cell Res. 2012;

608 30. Zhu S, Bhat S, Syan S, Kuchitsu Y, Fukuda M, Zurzolo C. Rab11a-Rab8a cascade regulates

609 the formation of tunneling nanotubes through vesicle recycling. J Cell Sci. 2018;

610 31. Kimura S, Hase K, Ohno H. The molecular basis of induction and formation of tunneling
611 nanotubes. Cell and Tissue Research. 2013.

612 32. Lou E, Fujisawa S, Morozov A, Barlas A, Romin Y, Dogan Y, et al. Tunneling nanotubes
613 provide a unique conduit for intercellular transfer of cellular contents in human
614 malignant pleural mesothelioma. PLoS One [Internet]. 2012 Mar 9 [cited 2021 Jun
615 16];7(3):33093. Available from: www.plosone.org

616 33. Fonville JM, Marshall N, Tao H, Steel J, Lowen AC. Influenza Virus Reassortment Is
617 Enhanced by Semi-infectious Particles but Can Be Suppressed by Defective Interfering
618 Particles. PLoS Pathog. 2015;

619 34. Jacobs NT, Onuoha NO, Antia A, Steel J, Antia R, Lowen AC. Incomplete influenza A virus
620 genomes occur frequently but are readily complemented during localized viral spread.
621 Nat Commun. 2019;

622 35. Phipps KL, Ganti K, Jacobs NT, Lee CY, Carnaccini S, White MC, et al. Collective
623 interactions augment influenza A virus replication in a host-dependent manner. Nat
624 Microbiol. 2020;

625 36. Crystal RG, Randell SH, Engelhardt JF, Voynow J, Sunday ME. Airway epithelial cells:
626 Current concepts and challenges. In: Proceedings of the American Thoracic Society
627 [Internet]. American Thoracic Society; 2008 [cited 2021 Jun 17]. p. 772–7. Available from:
628 /pmc/articles/PMC5820806/

629 37. Naphade S, Sharma J, Gaide Chevronnay HP, Shook MA, Yeagy BA, Rocca CJ, et al. Brief
630 reports: Lysosomal cross-correction by hematopoietic stem cell-derived macrophages via
631 tunneling nanotubes. Stem Cells [Internet]. 2015 Jan 1 [cited 2021 Jun 17];33(1):301–9.
632 Available from: https://pubmed.ncbi.nlm.nih.gov/25186209/

633 38. Jackson M V., Morrison TJ, Doherty DF, McAuley DF, Matthay MA, Kissenpfennig A, et al.
634 Mitochondrial Transfer via Tunneling Nanotubes is an Important Mechanism by Which
635 Mesenchymal Stem Cells Enhance Macrophage Phagocytosis in the In Vitro and In Vivo
636 Models of ARDS. Stem Cells [Internet]. 2016 Aug 1 [cited 2021 Jun 17];34(8):2210–23.
637 Available from: https://pubmed.ncbi.nlm.nih.gov/27059413/

638 39. Campana S, De Pasquale C, Carrega P, Ferlazzo G, Bonaccorsi I. Cross-dressing: An
639 alternative mechanism for antigen presentation [Internet]. Vol. 168, Immunology Letters.
640 Elsevier B.V.; 2015 [cited 2021 Jun 17]. p. 349–54. Available from:
641 https://pubmed.ncbi.nlm.nih.gov/26551033/

642 40. Xu W, Santini PA, Sullivan JS, He B, Shan M, Ball SC, et al. HIV-1 evades virus-specific IgG2
643 and IgA responses by targeting systemic and intestinal B cells via long-range intercellular
644 conduits. Nat Immunol [Internet]. 2009 [cited 2021 Jun 17];10(9):1008–17. Available
645 from: https://pubmed.ncbi.nlm.nih.gov/19648924/

646 41. Kongsomros S, Manopwisedjaroen S, Chaopreecha J, Wang SF, Borwornpinyo S,
647 Thitithanyanont A. Rapid and efficient cell-to-cell transmission of avian influenza h5n1
648 virus in mdck cells is achieved by trogocytosis. Pathogens [Internet]. 2021 Apr 16 [cited
649 2021 Jun 28];10(4):483. Available from: https://doi.org/10.3390/pathogens10040483

650 42. Gallagher ME, Brooke CB, Ke R, Koelle K. Causes and consequences of spatial within-host
651 viral spread. Viruses. 2018.

652 43. Han J, Perez JT, Chen C, Andrade J, Manicassamy B, Han J, et al. Genome-wide CRISPR /
653 Cas9 Screen Identifies Host Factors Essential for Influenza Virus Replication. Cell Rep.
654 2018;23(2):596–607.

655 44. Neumann G, Watanabe T, Ito H, Watanabe S, Goto H, Gao P, et al. Generation of
656 influenza A viruses entirely from cloned cDNAs. Proc Natl Acad Sci U S A. 1999;

657 45. Cox RS, Dunlop MJ, Elowitz MB. A synthetic three-color scaffold for monitoring genetic
658 regulation and noise. J Biol Eng. 2010;

659 46. Bindels DS, Haarbosch L, Van Weeren L, Postma M, Wiese KE, Mastop M, et al. MScarlet:
660 A bright monomeric red fluorescent protein for cellular imaging. Nat Methods. 2016;

661 47. White MC, Steel J, Lowen AC. Heterologous Packaging Signals on Segment 4, but Not
662 Segment 6 or Segment 8, Limit Influenza A Virus Reassortment. J Virol. 2017;

663 48. Phipps KL, Marshall N, Tao H, Danzy S, Onuoha N, Steel J, et al. Seasonal H3N2 and 2009
664 Pandemic H1N1 Influenza A Viruses Reassort Efficiently but Produce Attenuated Progeny.
665 J Virol. 2017;

666 49. Wittwer CT, Reed GH, Gundry CN, Vandersteen JG, Pryor RJ. High-resolution genotyping
667 by amplicon melting analysis using LCGreen. Clin Chem. 2003;

668 50. Schindelin J, Arganda-Carreras I, Frise E, Kaynig V, Longair M, Pietzsch T, et al. Fiji: An
669 open-source platform for biological-image analysis. Nature Methods. 2012.

670 51. Manders EMM, Visser AE, Koppen A, De Leeuw WC, Van Liere R, Brakenhoff GJ, et al.
671 Four-dimensional imaging of chromatin dynamics during the assembly of the interphase
672 nucleus. Chromosom Res [Internet]. 2003 [cited 2021 Jun 11];11(5):537–47. Available
673 from: https://pubmed.ncbi.nlm.nih.gov/12971728/

674 52. Costes S V., Daelemans D, Cho EH, Dobbin Z, Pavlakis G, Lockett S. Automatic and
675 quantitative measurement of protein-protein colocalization in live cells. Biophys J
676 [Internet]. 2004 [cited 2021 Jun 11];86(6):3993–4003. Available from:
677 https://pubmed.ncbi.nlm.nih.gov/15189895/

678 53. Bolte S, Cordelières FP. A guided tour into subcellular colocalization analysis in light
679 microscopy [Internet]. Vol. 224, Journal of Microscopy. Blackwell Publishing Ltd; 2006
680 [cited 2021 Jun 11]. p. 213–32. Available from:
681 https://onlinelibrary.wiley.com/doi/full/10.1111/j.1365-2818.2006.01706.x

682 54. Motulsky H. Analyzing Data with GraphPad Prism. PRism. 1999.

683 **Figure Legends:**

684 **Figure 1. IAV vRNPs associate with Rab11a within F-Actin rich TNTs.**

685 (A) MDCK cells, (B) A549 WT and (C) A549 Rab11a KO cells were mock-infected or infected with
686 NL09 or P99 viruses. Cells were stained for DAPI (blue), NP (red), Rab11a (green) and F-Actin
687 (pink). Representative images are shown with additional images in Supplementary Figure 1 (S1
688 A, B and C). Scale bar is 20µm for all images.

689 **Figure 2. IAV vRNPs co-localize with Rab11a within TNTs.**

690 (A) A549 WT and Rab11a KO cells were infected with NL09 viruses. Cells were stained for DAPI
691 (blue), NP (red), Rab11a (green) and F-Actin (grey). Representative confocal images are shown
692 with the high-resolution STED images depicted in the insets. The arrows depict the co-localized
693 puncta of NP and Rab11a. (B) Co-localization coefficient of NP and Rab11a within TNTs from
694 A549 WT and Rab11a KO cells (n=10 TNTs). Significance of differences in co-localization
695 between the WT and KO cells was tested using a two tailed unpaired t-test (**** P-value
696 <0.0001). (C) A549 WT cells were mock infected or infected with NL09 viruses and the
697 percentage of TNTs formed between 50 cell pairs were counted manually as NP+Rab11a+
698 (blue), NP-Rab11a+ (magenta) and NP+Rab11a- (teal). Error bars represent the SEM of two
699 biological replicates.

700 **Figure 3. Rab11a does not modulate TNT formation.**

701 A549 WT and Rab11a KO cells were mock infected or infected with NL09 viruses and the total
702 number of TNTs formed between 50 cell pairs were counted manually. Significance of
703 differences in the number of TNTs between mock and NL09 infected groups was tested using 1-
704 way ANOVA (** P-value <0.01). Error bars represent the SEM of two biological replicates.

705 **Figure 4. Disruption of actin or loss of Rab11a abrogates direct cell-cell transmission of**
706 **infection.**

707 MDCK cells infected with NL09 ΔHA Venus WT (A) or P99 ΔHA Venus WT (B) at a MOI of 0.5
708 were counted as single infected cells or foci of infected cells. Significance of differences in the
709 number of infected foci between the control and Cytochalasin D treated groups was tested
710 using 2-way ANOVA with Bonferroni's correction for multiple comparisons (**** P-value

711 <0.0001). Error bars represent the standard error of three biological replicates. A549 WT or
712 A549 Rab11a KO cells infected with NL09 ΔHA Venus WT (C) or P99 ΔHA Venus WT (D) at a MOI
713 of 0.5 were counted as single infected cells or foci of infected cells. Significance of differences in
714 the number of infected foci between cell types was tested using 2-way ANOVA with
715 Bonferroni's correction for multiple comparisons (**** P-value <0.0001). Error bars represent
716 the standard error of three biological replicates.

717 **Figure 5. Virion-independent genome transfer leads to productive infection by an actin-**
718 **dependent mechanism.**

719 (A) Experimental workflow for MDCK, A549 WT or A549 Rab11a KO infection and co-culture
720 with MDCK WSN HA cells (generated via BioRender.com). Plotted is the infectious virus yield
721 from co-culture of MDCK WSN HA cells with MDCK cells infected with NL09 ΔHA Venus WT and
722 NL09 ΔHA Scarlet VAR viruses either treated with Cytochalasin D (B) or Nocodazole (D). (C)
723 Infectious virus yield from MDCK cells infected with NL09 viruses and treated with Cytochalasin
724 D. (E) Infectious virus yield from co-culture of MDCK WSN HA cells with A549 WT or Rab11a KO
725 cells infected with either NL09 ΔHA Venus WT or NL09 ΔHA Scarlet VAR viruses. Significance of
726 differences between the control and Cytochalasin D or Nocodazole treated cells or between WT
727 and KO cells was tested using 2-way ANOVA with Bonferroni's correction for multiple
728 comparisons (* P-value <0.1; ** P-value <0.01; *** P-value <0.001; **** P-value <0.0001;
729 ns=not significant). Error bars represent the SEM of two biological replicates, each comprising
730 three replicate infections (black circles). The dotted line represents the limit of detection of the
731 plaque assay.

732 **Figure 6. TNTs allow for bidirectional shuttling of Rab11a between cells.**

733 (A) A549 Rab11a KO cells were infected with NL09 viruses and mixed with A549 WT cells pre-
734 stained with CellTracker Blue CMAC dye (blue). Cells were stained for NP (red), Rab11a (green)
735 and F-Actin (grey). Representative confocal image is shown with the high-resolution STED
736 images depicted in the inset. (B) Co-localization coefficient of NP and Rab11a within TNTs
737 formed between A549 WT and Rab11a KO cells (n=10 TNTs). Error bars represent the SEM.

738 **Figure 7. TNTs serve as conduits for genome mixing and reassortment in a Rab11a dependent**
739 **manner.**

740 Genotypes of clonal viral isolates collected from the culture medium of NL09 ΔHA Venus WT
741 and NL09 ΔHA Scarlet VAR virus infected A549 WT cells (A) or A549 Rab11a KO cells (B) co-
742 cultured with MDCK WSN HA cells. Three technical replicate co-cultures per condition were
743 sampled serially at the time points indicated and 21 plaque isolates were analyzed per sample.
744 The origin of the gene segments, represented by the columns in each table, is denoted by the
745 colored boxes (blue = WT and red = VAR). The segments are in order PB2, PB1, PA, NP, NA, M
746 and NS moving from left to right. The white panels indicate samples where no plaques were
747 detected (ND = not detected).

748 **Figure 8. Working model for Rab11a mediated vRNP transport across TNTs.**

749 vRNP complexes synthesized within the nucleus are exported out and form Rab11a-vRNP
750 complexes. Two potential fates of these complexes are shown - the classical assembly and
751 egress pathway for production of progeny virions and transport of these complexes via TNTs to

752 an uninfected cell. A new infection is initiated in the recipient cell, resulting in progeny virion

753 production. Generated via BioRender.com.

Figure 1

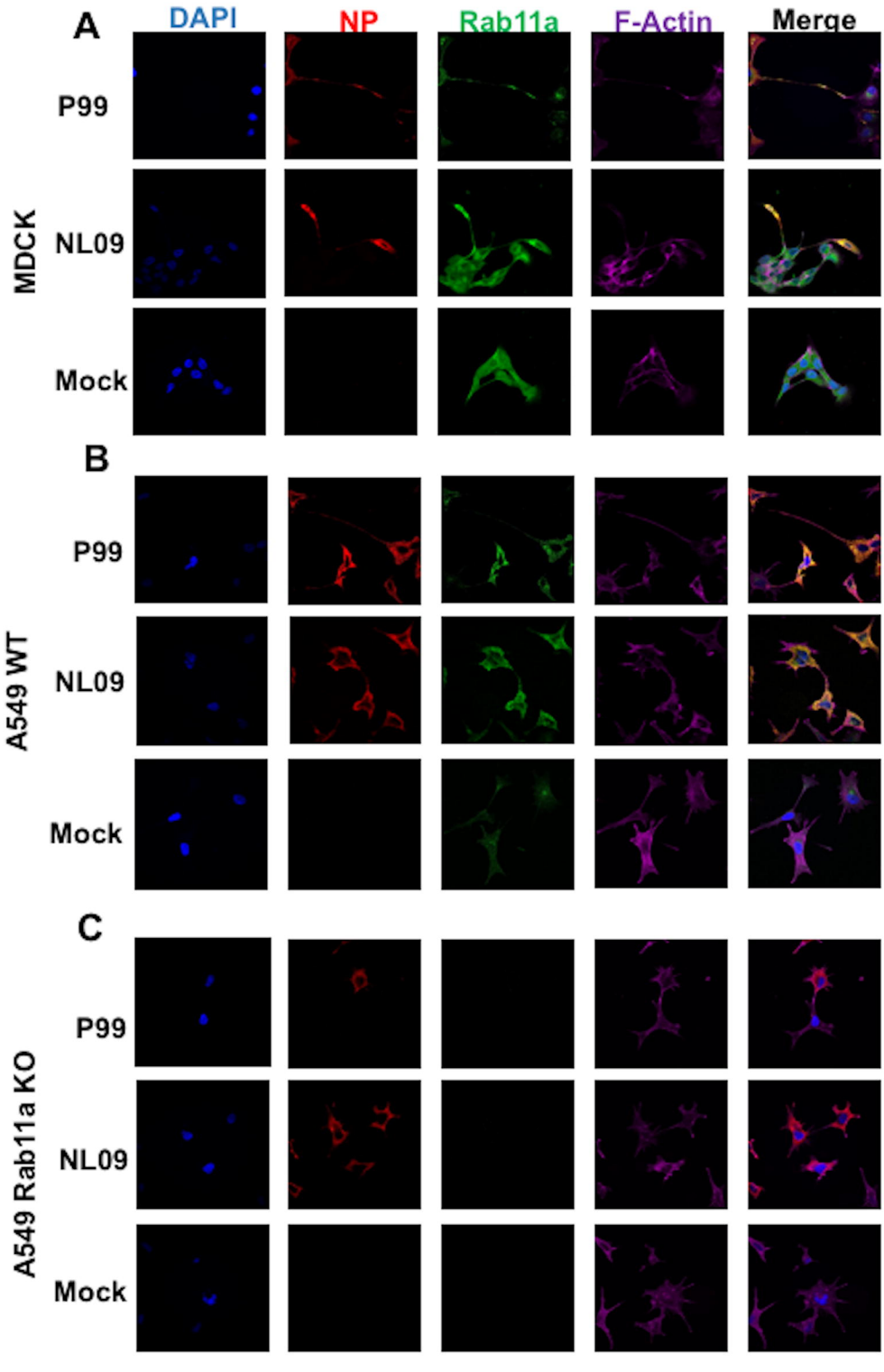
A
DAPI
NP
Rab11a
F-Actin
Merge
MDCK
P99
NL09
Mock
B
A549 WT
P99
NL09
Mock
C
A549 Rab11a KO
P99
NL09
Mock

Figure 2

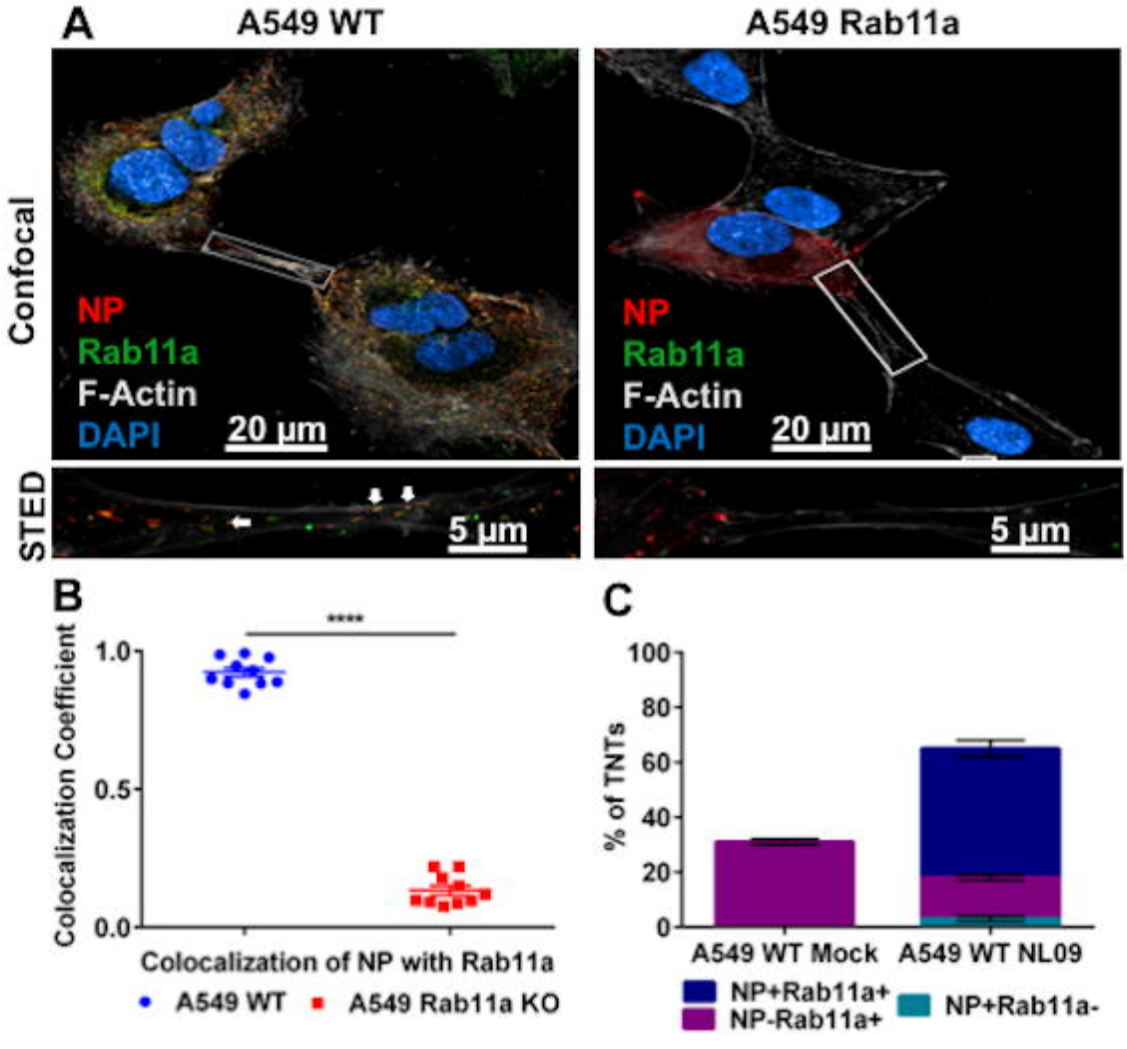
A
A549 WT
A549 Rab11a
Confocal
NP
Rab11a
F-Actin
DAPI
20 µm
STED
5 µm
B
****
Colocalization Coefficient
1.0
0.5
0.0
Colocalization of NP with Rab11a
A549 WT
A549 Rab11a KO
C
% of TNTs
100
80
60
40
20
0
A549 WT Mock
A549 WT NL09
NP+Rab11a+
NP-Rab11a+
NP+Rab11a-

Figure 3

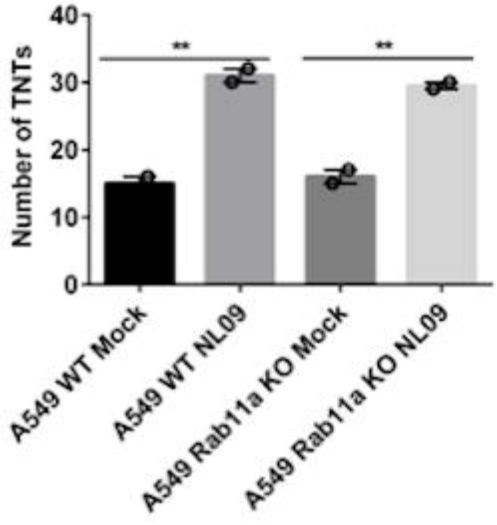
Number of TNTs
40
30
20
10
0
**
**
A549 WT Mock
A549 WT NL09
A549 Rab11a KO Mock
A549 Rab11a KO NL09

Figure 4

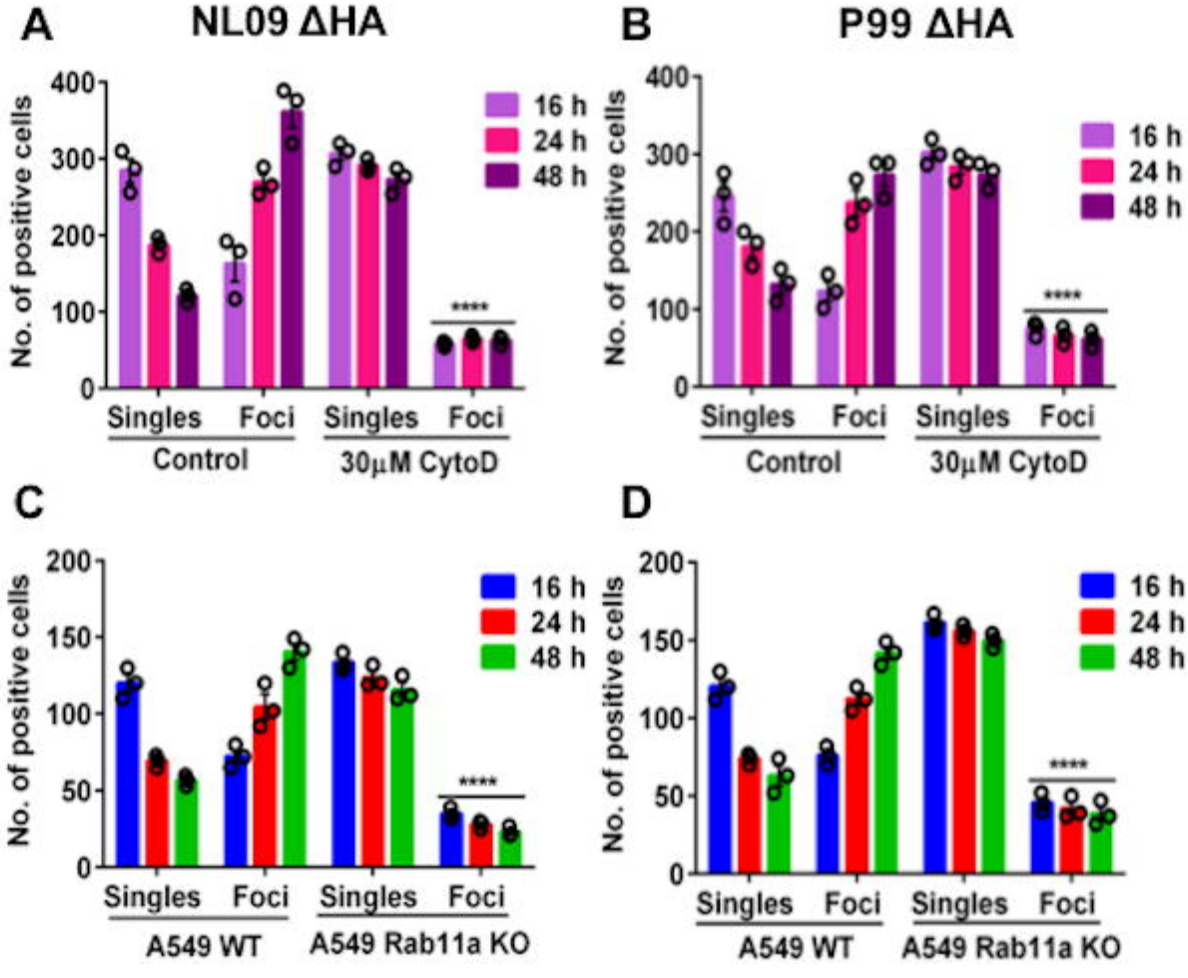
A
NL09 ΔHA
No. of positive cells
400
300
200
100
0
16 h
24 h
48 h
****
Singles
Foci
Singles
Foci
Control
30μM CytoD
B
P99 ΔHA
No. of positive cells
400
300
200
100
0
16 h
24 h
48 h
****
Singles
Foci
Singles
Foci
Control
30μM CytoD
C
No. of positive cells
200
150
100
50
0
16 h
24 h
48 h
****
Singles
Foci
Singles
Foci
A549 WT
A549 Rab11a KO
D
No. of positive cells
200
150
100
50
0
16 h
24 h
48 h
****
Singles
Foci
Singles
Foci
A549 WT
A549 Rab11a KO

Figure 5

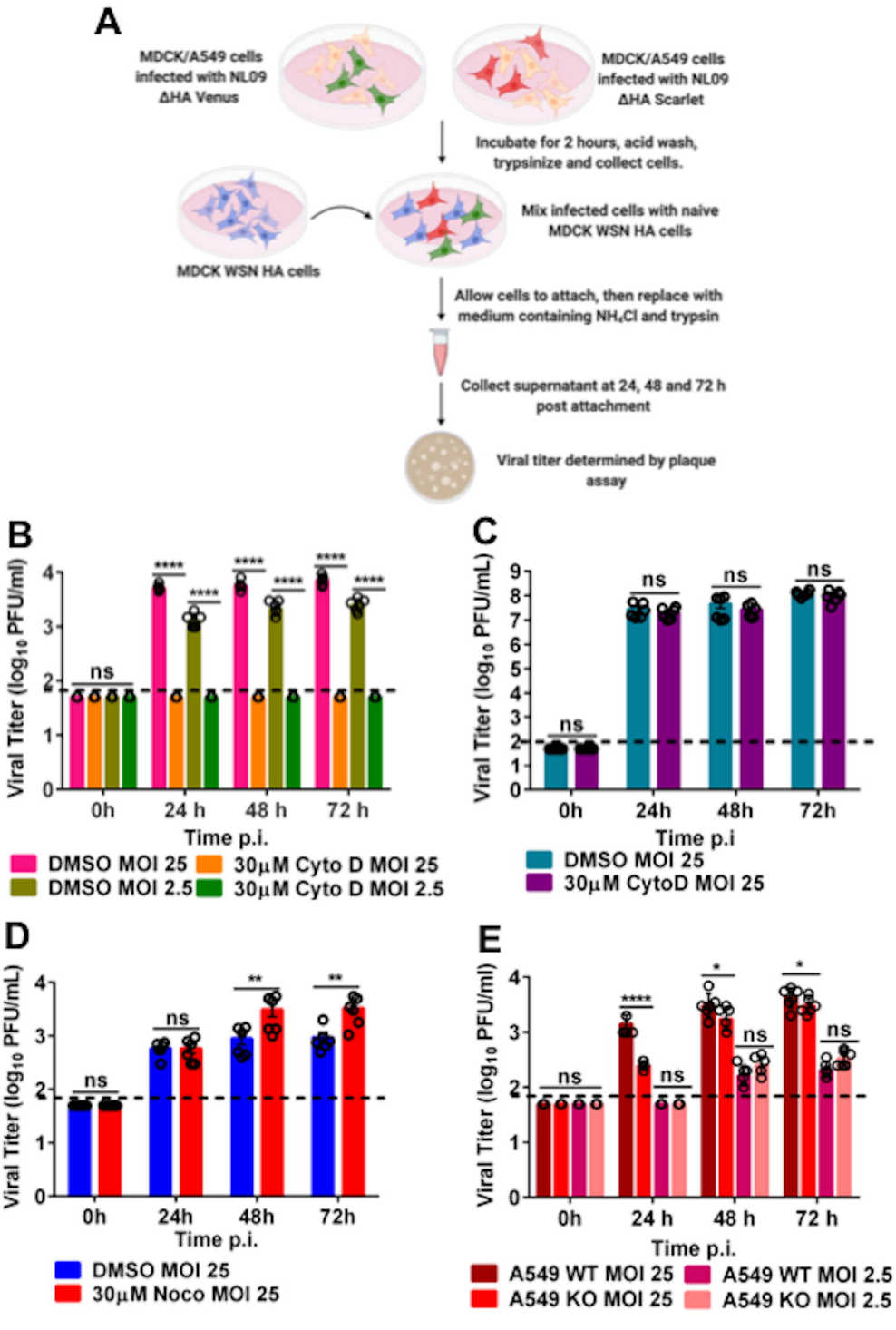
A
MDCK/A549 cells infected with NL09 ΔHA Venus
MDCK/A549 cells infected with NL09 ΔHA Scarlet
Incubate for 2 hours, acid wash, trypsinize and collect cells.
MDCK WSN HA cells
Mix infected cells with naive MDCK WSN HA cells
Allow cells to attach, then replace with medium containing NH4Cl and trypsin
Collect supernatant at 24, 48 and 72 h post attachment
Viral titer determined by plaque assay
B
Viral Titer (log10 PFU/ml)
Time p.i.
0h
24 h
48 h
72 h
ns
****
DMSO MOI 25
DMSO MOI 2.5
30μM Cyto D MOI 25
30μM Cyto D MOI 2.5
C
Viral Titer (log10 PFU/mL)
Time p.i
DMSO MOI 25
30μM CytoD MOI 25
D
Viral Titer (log10 PFU/mL)
Time p.i.
**
DMSO MOI 25
30μM Noco MOI 25
E
Viral Titer (log10 PFU/ml)
Time p.i.
*
A549 WT MOI 25
A549 KO MOI 25
A549 WT MOI 2.5
A549 KO MOI 2.5

Figure 6

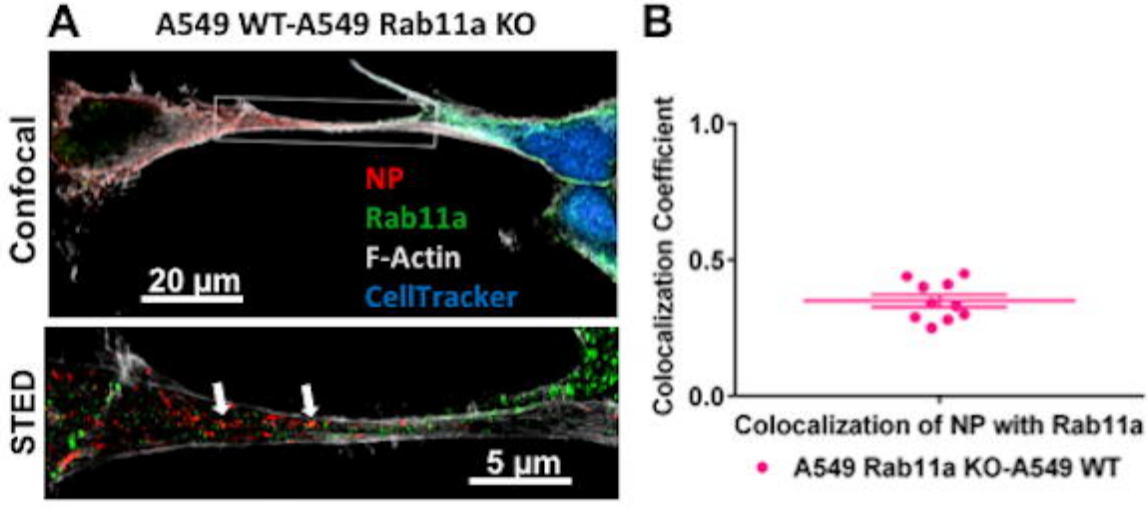
A
A549 WT-A549 Rab11a KO
Confocal
NP
Rab11a
F-Actin
CellTracker
20 µm
STED
5 µm
B
Colocalization Coefficient
1.0
0.5
0.0
Colocalization of NP with Rab11a
A549 Rab11a KO-A549 WT

Figure 7

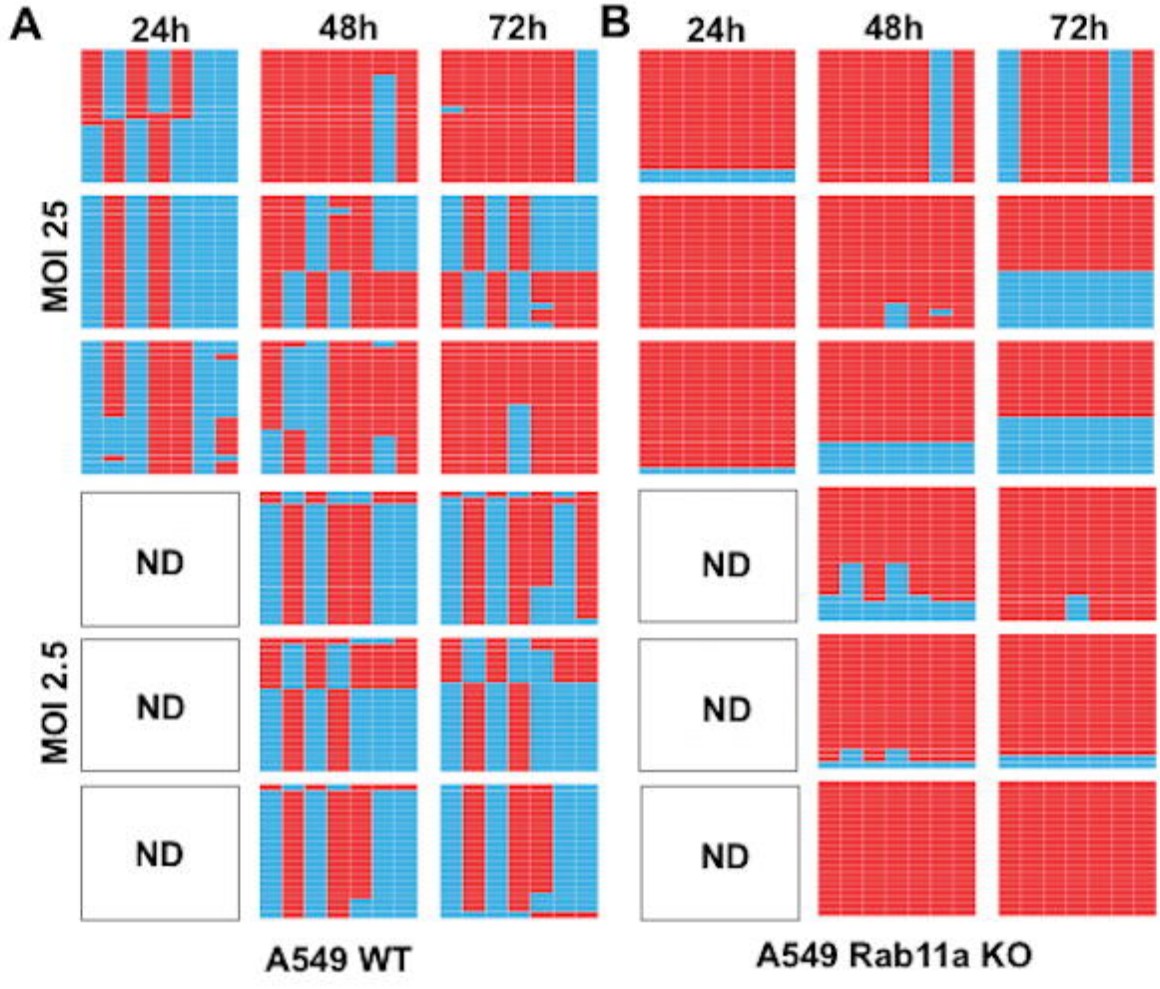
A
24h
48h
72h
B
24h
48h
72h
MOI 25
MOI 2.5
ND
ND
ND
ND
ND
ND
A549 WT
A549 Rab11a KO

Figure 8

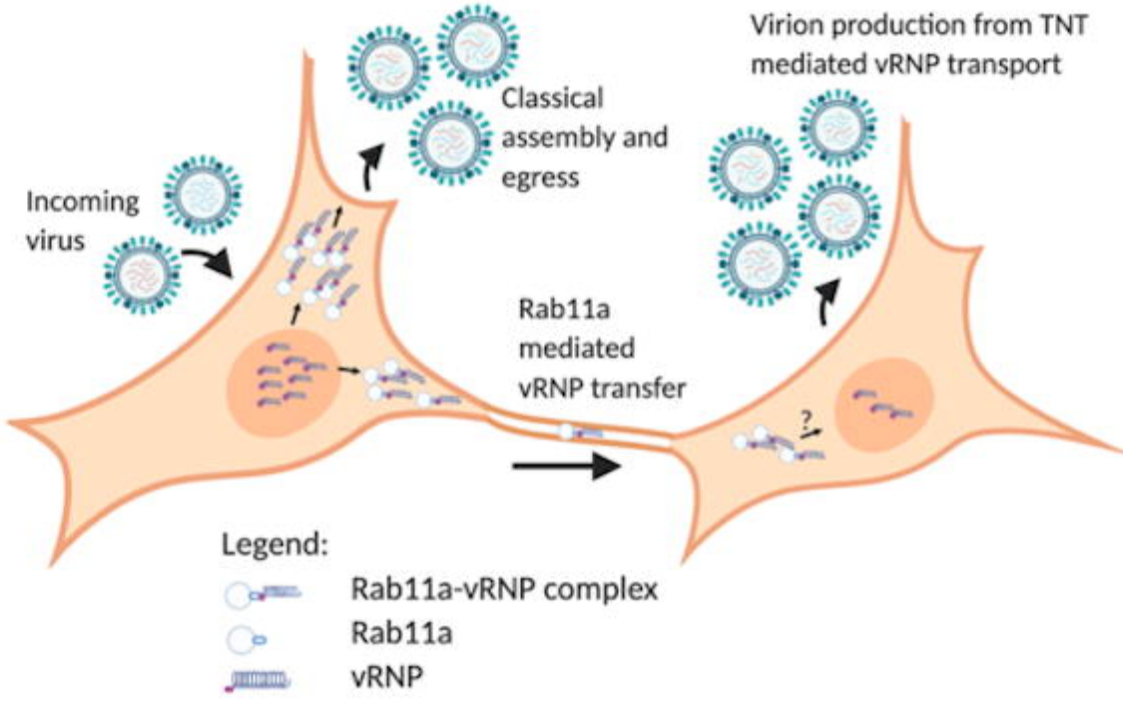
Incoming virus
Classical assembly and egress
Virion production from TNT mediated vRNP transport
Rab11a mediated vRNP transfer
?
Legend:
Rab11a-vRNP complex
Rab11a
vRNP